THE JOURNAL OF BIOLOGICAL CHEMISTRY VOL. 286, NO. 48, pp. 41656–41668, December 2, 2011

The Transition from Closed to Open Conformation of *Treponema pallidum* Outer Membrane-associated Lipoprotein TP0453 Involves Membrane Sensing and Integration by Two Amphipathic Helices*[S]

Received for publication, September 16, 2011, and in revised form, September 26, 2011 Published, JBC Papers in Press, September 30, 2011, DOI 10.1074/jbc.M111.305284

Amit Luthra[‡1], Guangyu Zhu[§1], Daniel C. Desrosiers[¶], Christian H. Eggers[‖], Vishwaroop Mulay[‡], Arvind Anand[‡], Fiona A. McArthur[‡], Fabian B. Romano[2], Melissa J. Caimano[‡], Alejandro P. Heuck[**‡‡], Michael G. Malkowski[§], and Justin D. Radolf[‡§§¶¶‖‖3]**

*From the Departments of [‡]Medicine, [§§]Pediatrics, [¶¶]Genetics and Developmental Biology, and [‖‖]Immunology, University of Connecticut Health Center, Farmington, Connecticut 06030, the [§]Hauptman-Woodward Medical Research Institute and Department of Structural Biology, State University of New York, Buffalo, New York 14203, the [¶]Section of Microbial Pathogenesis, Yale University School of Medicine, New Haven, Connecticut 06536, the [‖]Departments of Biomedical Sciences, Quinnipiac University, Hamden, Connecticut 06518, and the [‡‡]Department of Biochemistry and Molecular Biology, **Program in Molecular and Cellular Biology, University of Massachusetts, Amherst, Massachusetts 01003*

Background: TP0453 is the only lipoprotein in *T. pallidum* known to be associated with the outer membrane (OM).
Results: TP0453 adopts closed and open conformations; opening is associated with membrane sensing/insertion.
Conclusion: Two amphipathic helices are responsible for amphiphilic behavior of the molecule.
Significance: TP0453 is a novel bacterial lipoprotein whose amphiphilic behavior may contribute to *T. pallidum* OM biogenesis.

The molecular architecture and composition of the outer membrane (OM) of *Treponema pallidum* (*Tp*), the noncultivable agent of venereal syphilis, differ considerably from those of typical Gram-negative bacteria. Several years ago we described TP0453, the only lipoprotein associated with the inner leaflet of the *Tp* OM. Whereas polypeptides of other treponemal lipoproteins are hydrophilic, non-lipidated TP0453 can integrate into membranes, a property attributed to its multiple amphipathic helices (AHs). Furthermore, membrane integration of the TP0453 polypeptide was found to increase membrane permeability, suggesting the molecule functions in a porin-like manner. To better understand the mechanism of membrane integration of TP0453 and its physiological role in *Tp* OM biogenesis, we solved its crystal structure and used mutagenesis to identify membrane insertion elements. The crystal structure of TP0453 consists of an $\alpha/\beta/\alpha$-fold and includes five stably folded AHs. In high concentrations of detergent, TP0453 transitions from a closed to open conformation by lateral movement of two groups of AHs, exposing a large hydrophobic cavity. Triton X-114 phase partitioning, liposome floatation assay, and bis-1-anilino-8-naphthalenesulfonate binding revealed that two adjacent AHs are critical for membrane sensing/integration. Using terbium-dipicolinic acid complex-loaded large unilamellar vesicles, we found that TP0453 increased efflux of fluorophore only at acidic pH. Gel filtration and cross-linking experiments demonstrated that one AH critical for membrane sensing/insertion also forms a dimeric interface. Based on structural dynamics and comparison with *Mycobacterium tuberculosis* lipoproteins LprG and LppX, we propose that TP0453 functions as a carrier of lipids, glycolipids, and/or derivatives during OM biogenesis.

Syphilis is a multistage, sexually transmitted illness caused by the spirochetal pathogen *Treponema pallidum*, an extracellular, highly motile bacterium (1). Although syphilis is one of the oldest recognized sexually transmitted diseases, the mechanisms underlying its pathogenesis are poorly understood in large part because *T. pallidum* cannot be cultivated *in vitro* (2). The molecular architecture of the *T. pallidum* cell envelope is believed to be a primary determinant of the capacity of syphilis spirochete to evade the robust immune responses it elicits in its obligate human host, a property that has led to its designation as "the stealth pathogen" (1, 3). Like Gram-negative bacteria, *T. pallidum* has both outer and cytoplasmic membranes; however, the composition and physical properties of its cell envelope differ markedly from those of prototypical diderms (4, 5).

* This work was supported by Public Health Service Grants AI-26756 (to J. D. R.) and RG-71111-N (to A. P. H.). This work was also supported, in whole or in part, by National Institutes of Health Grants GM074899, GM094611, and GM094597 (NIGMS Protein Structure Initiative to the High throughput screening laboratory at the Hauptman Woodward Institute).
[S] The on-line version of this article (available at http://www.jbc.org) contains supplemental Tables 1–2 and Figs. 1–3.
The atomic coordinates and structure factors (codes 3K8G, 3K8H, 3K8J, and 3K8I) have been deposited in the Protein Data Bank, Research Collaboratory for Structural Bioinformatics, Rutgers University, New Brunswick, NJ (http://www.rcsb.org/).
[1] Both authors contributed equally to this work.
[2] Supported in part by National Institutes of Health National Research Service Award T32 GM08515.
[3] To whom correspondence should be addressed: Dept. of Medicine, The University of Connecticut Health Center, 263 Farmington Ave., Farmington, CT 06030-3715. Tel.: 860-679-8480; Fax: 860-679-1358; E-mail: JRadolf@up.uchc.edu.

The OM[4] of *T. pallidum* is devoid of lipopolysaccharide, contains phosphatidylcholine, phosphatidylserine, and uncharacterized glycolipids as its major lipid constituents, and is much more permeable to lipophilic compounds (6–9). In contrast to the OM of *Escherichia coli*, which contains a high density of integral β-barrel forming proteins, the OM of *T. pallidum* has a paucity of membrane-spanning proteins, often referred to collectively as rare OM proteins (4, 5, 10, 11). A major difference between the *E. coli* and *T. pallidum* cell envelopes relates to their lipoprotein components. In *T. pallidum,* with one known exception (described below), all lipoproteins that have been characterized to date have been localized to the periplasmic face of the inner membrane (5, 12, 13), whereas lipoproteins in *E. coli* are located predominantly at the periplasmic face of the OM (14).

Several years ago we devised a strategy for identifying OM-associated proteins in *T. pallidum* based upon the use of 3-(trifluoromethyl)-3-(*m*-[^{125}I]iodophenyl-diazarene) (15, 16). This highly lipophilic molecule stably partitions into the hydrocarbon core of a membrane where upon UV photoactivation it promiscuously binds to intramembranous components (15). Using this reagent in conjunction with Triton X-114 phase-partitioning (17), we detected a single strongly radiolabeled polypeptide of ~30 kDa (16), subsequently identified by peptide sequencing as TP0453 (p30.5) (18). Although this approach was intended to identify OM-spanning proteins, surprisingly, TP0453 was found to be a lipoprotein. Detailed investigation revealed, however, that TP0453 possesses unique physical properties in addition to being the only lipoprotein known to be localized to the *T. pallidum* OM. Whereas the polypeptide moieties of spirochetal lipoproteins typically are hydrophilic (19), the polypeptide portion of TP0453 is amphiphilic and was predicted to contain five AHs as membrane-insertion elements (18). Importantly, liposome incorporation assays revealed that non-lipidated p30.5 enhances the permeability of small unilamellar vesicles. Based on these results, we hypothesized that the polypeptide portion of native TP0453 exists in a dynamic equilibrium between OM-inserted and -uninserted forms and that transient perturbations in the OM caused by insertion of AHs facilitates ingress of water-soluble nutrients (18).

In the present study we solved the crystal structure of TP0453 and performed detailed physicochemical characterization of wild type (WT) and mutated forms of the protein to elucidate its contribution to the membrane biology of *T. pallidum*. We found that TP0453 is structurally dynamic, converting from a closed to an open form in the presence of high concentrations of nonionic detergent with concomitant exposure of a large hydrophobic cavity. As predicted, TP0453 possesses multiple AHs as part of its overall α/β/α-fold; however, only two adjacent AHs were found to be critical for membrane integration. In the closed form these helices contribute to a surface-exposed hydrophobic patch, which we hypothesize "senses" the membrane interior when the polypeptide is in proximity to the lipid bilayer. Assays using unilamellar vesicles (LUVs) confirmed the ability of the protein to enhance efflux of fluorophore but only under acidic conditions. Although a monomer as a major form in solution, TP0453 forms stable a dimer upon membrane insertion. The similarity between the structure of TP0453 and solved structures for two *Mycobacterium tuberculosis* lipoproteins, LprG and LppX (20, 21), suggests that TP0453 may function as a carrier of lipids, glycolipids, and/or derivatives during OM biogenesis in *T. pallidum*.

EXPERIMENTAL PROCEDURES

Propagation and Harvesting of T. pallidum—The animal protocol described in this work strictly follows the recommendations of the Guide for Care and Use of Laboratory Animals of the National Institutes of Health and was approved by the University of Connecticut Health Center Animal Care Committee under the auspices of Animal Welfare Assurance A347-01. The Nichols-Farmington strain of *T. pallidum* subspecies pallidum was propagated by intratesticular inoculation of adult New Zealand White rabbits with 1×10^8 treponemes per testis and harvested aseptically ~10 days later (13). To remove rabbit testicular debris, the treponemal suspension was transferred to a sterile tube and centrifuged for 10 min at 500 × g. *T. pallidum* was enumerated using a Petroff-Hausser counting chamber (Hausser Scientific Company, Horsham, PA). The treponemes were sedimented by centrifugation for 20 min at 10,000 × *g* at 4 °C, and the pellet was washed with ice-cold phosphate-buffered saline (PBS) before processing for blue native polyacrylamide gel (BN-PAGE) (see below).

Cloning and Mutagenesis—The cloning of *tp0453* into the expression vector pET4341 has been described elsewhere (18). pET4341::TP0453 encodes a glutathione *S*-transferase-hexahistidine chimera with a thrombin cleavage site fused to the N terminus of TP0453 lacking a signal peptide (*i.e.* residues 27–287). The TP0453 coding sequence in pET4341::TP0453 was mutated with a site-directed mutagenesis kit (Agilent Technologies, Santa Clara, CA) using the primers listed in supplemental Table 1. The *ompF* gene (without the signal sequence-encoding portion) was PCR-amplified from *E. coli* DNA using the primers listed in supplemental Table 1 and cloned into the NheI (5′-end) and HindIII (3′-end) restriction sites of pET23b (Novagen, San Diego, CA). All constructs were verified by nucleotide sequencing.

Purification and Selenomethionine Labeling of TP0453—For crystallographic studies, a 4-liter culture of Luria-Bertani (LB) was inoculated with 25 ml of an overnight culture of pET4341:TP0453 in Rosetta (DE3) cells (EMD Chemicals, Gibbstown, NJ) grown at 37 °C. At an $A_{600\ nm}$ of 0.6, isopropyl β-D-1-thiogalactopyranoside was added to a final concentration of 0.5 mM; the cells were grown for an additional 3 h and then harvested by centrifugation at 6000 × *g* for 30 min at 4 °C. The pellets were suspended with 20 ml of 50 mM Tris (pH 7.5), 10% glycerol, 100 μg of lysozyme (Sigma), and 100 μl of protease inhibitor mixture (Sigma) and lysed by sonication. The sonicated lysate was centrifuged at 20,000 × *g* for 30 min at 4 °C followed by filtra-

[4] The abbreviations used are: OM, outer membrane; TP, *T. pallidum;* AHs, amphipathic helices; LUV, large unilamellar vesicle; SHP, surface hydrophobic patch; ANS, anilino-8-naphthalenesulfonate; BN-PAGE, blue native PAGE; β-OG, *n*-octyl-β-D-glucopyranoside; Tricine, *N*-[2-hydroxy-1,1-bis(hydroxymethyl)ethyl]glycine; Bis-Tris, 2-[bis(2-hydroxyethyl)-amino]-2-(hydroxymethyl)propane-1,3-diol; $Tb(DPA)_3^{3-}$, terbium dipicolinic acid complex.

tion through a 0.22 μM filter before loading onto a 5-ml nickel-nitrilotriacetic acid column equilibrated with 50 mM Tris (pH 7.5), 100 mM NaCl, 10 mM imidazole (Buffer A). The column initially was washed with Buffer A alone and subsequently twice with Buffer A containing 20 mM and then 40 mM imidazole. The protein was eluted with 50 ml of 50 mM Tris (pH 7.5), 100 mM NaCl, 400 mM imidazole (Buffer B) in 10-ml fractions, and the fractions containing eluted proteins were pooled. Pooled fractions from nickel-nitrilotriacetic acid column were mixed with pre-swollen glutathione-agarose beads and incubated overnight at 4 °C. The following day the glutathione-agarose with bound protein was loaded onto an empty column and washed extensively with 50 mM Tris (pH 7.5), 100 mM NaCl, and 10% glycerol. To excise the N-terminal GST tag, 100 units of thrombin were added to the resin followed by incubation for 12–14 h at 22 °C on a shaker. Cleaved TP0453 in the flow-through was loaded onto a cation exchange column packed with SP-Sepharose (Bio-Rad) and washed extensively with 25 mM Tris (pH 7.5), 10% glycerol, and eluted with a gradient of 0–1.0 M NaCl. Fractions containing TP0453 were pooled and subjected to size exclusion chromatography using Superdex 75 HR 10/300 column (GE Healthcare) equilibrated with 50 mM Tris (pH 7.5), 100 mM NaCl. All mutants (supplemental Table 1) were expressed and purified using the same protocol. The ProtParam tool provided by the ExPASy proteomics server (22) was used to calculate the molar extinction coefficient (M^{-1} cm^{-1}) of the proteins. To generate selenomethionine-substituted TP0453, pET4341:TP0453 was transformed into *E. coli* B834 (Emd Chemicals), and a single colony was inoculated into 100 ml of M9 minimal medium supplemented with 50 μg/ml ampicillin. 25-ml aliquots of overnight culture were inoculated into 1 liter of M9 minimal medium, which then was incubated at 37 °C to an $A_{600\ nm}$ of 0.6. Each 1-liter culture was then directly supplemented with a mixture of the following amino acids: 100 mg of lysine, phenylalanine, and threonine, 50 mg of isoleucine, leucine, and valine, and 60 mg of selenomethionine. The purification procedure for selenomethionine-incorporated TP0453 was the same as that used for the native protein.

Crystallization and Data Collection—Initial crystallization screening was carried out in the High Throughput Crystallization Laboratory at the Hauptman-Woodward Medical Research Institute utilizing a sparse-matrix screen designed for soluble proteins and a tailored grid screen optimized for membrane proteins that is based on detergent phase partitioning (23, 24). A 1536 mixture screen utilizing the microbatch-under-oil method was set up with purified TP0453 in 25 mM Tris (pH 7.2), 150 mM NaCl containing 0.15% (w/v) *n*-octyl-β-D-glucopyranoside (β-OG) at a protein concentration of 8.2 mg/ml. One crystallization lead generated from the tailored membrane protein screen was further optimized to generate the crystals utilized in this study. Specifically, crystals were grown at 20 °C in sitting drops by combining 2 μl of protein solution with 2 μl of 10–15% polyethylene glycol 3350 (PEG 3350), 100 mM $MgCl_2$, 100 mM MES (pH 5.5), and 0–1.0% (w/v) β-OG. Different crystal morphologies were observed depending on the concentration of β-OG utilized in the crystallization setup. Two different crystal morphologies were observed when concentrations of β-OG between 0–0.5% (w/v) were utilized; two additional morphologies were observed when concentrations of β-OG were used between 0.5 and 0.75% (w/v) and between 0.75 and 1.0% (w/v), respectively. We designated the different crystal morphologies as Forms I-IV with Forms I and II generated from low concentrations of β-OG (0–0.5%) and Forms III and IV generated from high concentrations of β-OG (0.75–1.0%). Forms I and II were cryopreserved by initial transfer to a solution consisting of 15% PEG 3350, 100 mM $MgCl_2$, 100 mM MES (pH 5.5) followed by subsequent transfers to solutions containing increasing concentrations of 2-methyl-2, 4-pentanediol up to a final concentration of 15% (w/v). Forms III and IV were cryopreserved via direct transfer to a solution consisting of 15% PEG 3350, 100 mM $MgCl_2$, 100 mM MES (pH 5.5), 5% (w/v) glycerol, and 5% (w/v) ethylene glycol. After incubation in cryoprotectant, the crystals were looped and flash-cooled directly into the N_2 gas stream before diffraction analysis. Crystals of the selenomethionine derivative of TP0453 were produced using the same techniques, generating a crystal morphology corresponding to Form III. Data were collected for Forms I, II, and IV on beamline A1 at the Cornell High Energy Synchrotron Source (Ithaca, NY) using an Area Detector Systems CCD Quantum-210 detector. For Form III, both native and selenomethionine multiwavelength anomalous diffraction data sets were collected on beamline 9-2 at the Stanford Synchrotron Research Laboratory (Menlo Park, CA) using remote data collection techniques (25). Data sets were measured at the selenium K-edge peak (0.97915 Å), inflection point (0.97932 Å), and remote (0.96396 Å) energy wavelengths using a MarMosaic-325 CCD detector. All data were processed and scaled using the HKL2000 program suite (26). Details of the data collection statistics are summarized in Table 1.

Structure Solution and Refinement—The structure of Form III was solved using multiwavelength anomalous diffraction phasing techniques. All three expected selenium sites were located using the program SHELX (27). The program SHARP (28) was used to further refine the heavy atom substructure and for density modification. The figure of merit was 0.48 after substructure refinement, with a subsequent increase to 0.75 after density modification. The program ARP/wARP (29) was utilized to generate an initial model for the TP0453 structure, comprising 141 of the 260 residues (54% total). At this stage 10 β-strands and 6 α-helices were identifiable. The remaining residues were built manually by performing iterative cycles of refinement and model building using the programs REFMAC (30) and COOT (31), respectively. The structures of Forms I, II, and IV were solved by molecular replacement using the program PHASER (32) and the structure of Form III as the search model. Iterative cycles of model building using COOT and refinement using REFMAC5 were performed to generate the final models for Forms I, II, and IV. Water molecules were added, and TLS refinement (33) was carried out on each crystal form in the final rounds of REFMAC5 refinement. Final refinement statistics are summarized in Table 1. All figures were made using PyMOL including hydrophobic (VASCo plugin) (34). The PISA program

(35) was used to calculate the possible oligomeric assembly of all four crystal forms.

Expression and Purification of OmpF—OmpF was expressed in the BL21 (DE3) Rosetta-gami strain (Agilent Technologies). For OmpF purification, a 1-liter culture of LB was inoculated with 25 ml of overnight culture grown of (pET23b:*ompF*) at 37 °C. At an $A_{600\ nm}$ of 0.6, isopropyl β-D-1-thiogalactopyranoside was added to the culture to a final concentration of 0.3 mM. Cells were grown for an additional 3 h and then harvested by centrifugation at 6000 × *g* for 30 min at 4 °C. The pellets were resuspended with 20 ml of 50 mM Tris (pH 7.5), 100 mg of lysozyme, and 100 ml of protease inhibitor mixture, and the bacterial suspension was lysed by sonication. The pellet was recovered by centrifugation at 20,000 × *g* for 30 min at 4 °C and then incubated in solubilization buffer (50 mM Tris (pH 7.0), 8 M urea) for 30 min at 4 °C; the remaining insoluble material was removed by centrifugation at 20,000 × *g* for 30 min at 4 °C. The supernatant was added to a Q-Sepharose column equilibrated with solubilization buffer and was washed with wash buffer (50 mM Tris (pH 7.0), 8 M urea). Bound protein was eluted off the column using a linear gradient of NaCl from 0 to 0.5 M. Purified protein was incubated in folding buffer (0.5% *n*-dodecyl-β-D-glucopyranoside, 0.5% *n*-dodecyl-β-D-maltoside, 100 mM NaCl, 50 mM Tris) for 24 h at 4 °C to ensure complete folding of the protein. The samples were centrifuged at 20,000 × *g* for 30 min at 4 °C to remove misfolded aggregates.

Preparation of Liposomes—All phospholipids were purchased from Avanti Polar Lipids (Alabaster, AL). Large LUVs were generated using an Avanti Mini-Extruder. A mixture of 1-palmitoyl-2-oleoyl-*sn*-glycero-3-phosphocholine, 1-palmitoyl-2-oleoyl-*sn*-glycero-3-[phospho-L-serine] (sodium salt), 1-palmitoyl-2-oleoyl-*sn*-glycero-3-[phospho-(racemic)-glycerol] (sodium salt), and 1,2-dioleoyl-*sn*-glycero-3-phosphoethanolamine (69.3:17:13:0.7 mol %, respectively) in chloroform was dried at room temperature under argon and kept in vacuum for at least 4 h. This ratio simulates the phospholipid composition of the *T. pallidum* OM (7). To hydrate the lipid mixture, 0.5 ml of 50 mM HEPES (pH 7.5), 100 mM NaCl was added to the dried phospholipids, and the sample was incubated for 30 min at 37 °C. The lipids were resuspended by vortexing and then passed 21 times at 23 °C through the extruder equipped with a 100-nm pore size polycarbonate filter. The filter dictates the final size of the vesicles (mean diameter ~110 nm) and reduces the chances of contamination with larger particles or foreign material. The resulting liposomes were stored at 4 °C for 2 weeks. Liposomes containing $Tb(DPA)_3^{3-}$ were prepared as above except that buffer A, including 3 mM terbium(III) chloride ($TbCl_3$) and 9 mM 2,6-pyridinedicarboxylic acid (Sigma) neutralized to pH 7 was added to the lipid film. The suspended phospholipid mixtures were frozen in liquid N_2 and thawed at 37 °C a total of 6 times to reduce the number of multilamellar liposomes and to enhance the trapped volumes of the vesicles. Loaded liposomes were separated from non-encapsulated $Tb(DPA)_3^{3-}$ by gel filtration using Superdex ™ 75 (GE Healthcare) in 50 mM HEPES (pH 7.5), 100 mM NaCl.

Circular Dichroism Spectroscopy—CD measurements were carried out using a Jasco J-715 spectropolarimeter (Jasco, Easton, MD), and the results were expressed as relative ellipticity. The CD spectra were obtained at protein concentrations of 10 μM in 50 mM Tris (pH 7.5), 100 mM NaCl in a 1-mm cell at 25 °C. The values obtained were normalized by subtracting the base line recorded for the buffer having the same concentration of NaCl under similar conditions. Deconvolution of the CD data was performed using the DICHROWEB server (36).

Immunologic Reagents—Rat polyclonal antiserum directed against TP0453 was described previously (18). A mouse monoclonal antibody (hybridoma clone HIS-1) specific for polyhistidine tags was purchased from Sigma.

SDS-PAGE and Immunoblot Analysis—Samples were resolved by 10% SDS-PAGE and transferred to nitrocellulose membranes (0.45 μM pore size, GE Healthcare) at 25 V for 30 min using a semidry apparatus (Bio-Rad). Membranes were blocked for 1 h with PBS, 5% nonfat dry milk, 5% fetal bovine serum, and 0.1% Tween 20 and probed overnight at 4 °C with primary antibodies at dilutions of 1:3000 (anti-TP0453) or 1:1000 (anti-His tag). After washing with PBS and 0.05% Tween 20 (PBST), the membranes were incubated for 1 h at 4 °C with horseradish peroxidase-conjugated goat anti-rat or anti-mouse antibodies (Southern Biotech, Birmingham, AL) at a dilution of 1:30,000. After additional washes with PBST, the immunoblots were developed using the SuperSignal West Pico chemiluminescent substrate (Thermo Fisher Scientific).

Triton X-114 Phase Partitioning—10 μg of each protein were incubated in 250 μl of PBS containing 2% Triton X-114 (Sigma) and 0.005% protease inhibitor mixture (Sigma) and diluted with 990 μl of PBS. After incubation for 1 h at 4 °C, each sample was dialyzed overnight against PBS at 4 °C. After dialysis, the samples were incubated at 37 °C for 10 min followed by centrifugation at 20,000 × *g* for 20 min at 4 °C. After centrifugation, the aqueous and detergent phases were separated, and both phases were washed 5 times. All washed samples were precipitated with 10 volumes of acetone overnight at −80 °C for subsequent SDS-PAGE and immunoblot analysis.

Liposome Floatation Assay—WT and mutant proteins (300 nM final concentration) were incubated with ~100 μg of LUVs for 1 h at 22 °C in low (50 mM Tris (pH 7.5), 100 mM NaCl) and high salt (50 mM Tris (pH 7.5), 1.0 M NaCl) buffers. Incorporation was terminated by adding sucrose to a final concentration of 50%, and the mixtures were transferred to an ultracentrifuge tube. Discontinuous sucrose gradients were made by gently adding layers of 40 and 6% sucrose to the ultracentrifuge tubes. After centrifugation at 90,000 × *g* for 1 h at 4 °C, the liposome (top layer)- and non-liposome (middle and bottom layers)-containing fractions were carefully removed.

Pore Formation Assay—For end-point measurements, liposomes loaded with $Tb(DPA)_3^{3-}$ were diluted to a final lipid concentration of 100 μM at the different pH values using buffer 50 mM Tris (pH 7.5), 100 mM NaCl supplemented with 5 mM EDTA. The net initial emission intensity (F_0) was determined after equilibration of the sample at 25 °C for 5 min. Aliquots of TP0453 or OmpF were added to the liposome suspension at 100 nM final concentration, and samples were incubated for 30 min at 37 °C. After re-equilibration to 25 °C, the final net emission intensity (F_f) of the sample was determined (*i.e.* after blank subtraction and dilution correction) and the fraction of $Tb(DPA)_3^{3-}$ quenched was estimated using F_f/F_0. For kinetic measurements,

TABLE 1
Crystallographic data collection and refinement statistics
r.m.s.d., root mean square deviations; MPD, 2-methyl-2,4-pentanediol.

Crystallographic Parameter	Form I	Form II	Form III	Form IV	Form III peak	Form III inflection	Form III high remote
PDB ID	3K8G	3K8H	3K8J	3K8I			
Space group	$P2_12_12$	C2	$P2_12_12$	$P2_12_12$	$P2_12_12$	$P2_12_12$	$P2_12_12$
No. in ASU	2	2	1	1	1	1	1
Unit cell (Å)							
a	87.74	145.30	45.68	45.42	45.78	45.79	45.80
b	159.87	44.76	157.51	143.73	157.66	157.78	157.77
c	44.53	96.97	43.03	42.92	43.03	43.04	43.04
$\alpha = \beta = \gamma$ (°)	90.00	$\beta = 99.75$	90.00	90.00	90.00	90.00	90.00
Wavelength (Å)	0.9789	0.9789	1.000	0.9789	0.97915	0.97932	0.96396
Resolution (Å)	50-1.95	50-2.40	50-2.20	40-2.20	50-2.50	50-2.50	50-2.50
Res. last shell (Å)	2.02-1.95	2.44-2.40	2.28-2.20	2.24-2.20	2.59-2.50	2.59-2.50	2.59-2.50
R_{merge}	6.2 (45.5)	6.2 (30.3)	4.7 (27.0)	5.6 (19.1)	7.4 (32.5)	6.7 (30.3)	6.6 (30.5)
Total observations	224,026	93,295	114,578	83,000	108,167	53,671	53,397
Total unique	46,264	24,202	16,362	14,662	11,484	11,464	11,444
$I/\sigma(I)$	23.3 (3.4)	19.6 (3.1)	43.9 (6.8)	29.6 (4.5)	42.9 (3.9)	31.8 (2.9)	30.9 (3.1)
Completeness (%)	99.9 (100)	98.1 (82.7)	98.6 (88.4)	98.8 (89.9)	85.4 (48.8)	82.8 (37.8)	82.0 (39.1)
Multiplicity	4.8	3.9	7.0	5.7	11.0	5.7	5.7
Wilson B factor (Å^2)	27.6	46.8	36.3	38.6			
Atoms in refinement	4,116	4,112	2,118	2,041			
R_{work}	21.5	20.6	21.2	22.8			
R_{free}	25.4	25.8	26.0	27.1			
Waters and ligand	213	129	122	77			
MPD	4	2	0	0			
Average B factor, protein (Å^2)	41.3	48.0	45.2	56.2			
Average B factor, solvent (Å^2)	34.6	37.0	38.6	39.3			
Mean positional error (Å)	0.166	0.401	0.261	0.307			
r.m.s.d., bond length (Å)	0.014	0.010	0.010	0.009			
r.m.s.d., bond angle (°)	1.45	1.24	1.19	1.21			

the same procedure was used with the difference that F_f was monitored continuously right after TP0453 or OmpF addition at 25 °C, and F_f/F_0 was plotted as a function of time.

Bis-ANS Binding Kinetics—1 μM concentrations of each sample in 50 mM Tris (pH 7.5), 50 mM NaCl was stirred in a 1-cm path length cuvette. Subsequently, graded aliquots (1–25 μM final concentration) of bis-ANS (Sigma) were added to the cuvette, and the excitation wavelengths were set to 390 nm. The emission spectra were collected from 400 to 600 nm in a Hitachi F-2500 fluorescence spectrophotometer. For each measurement, the fluorescence intensity was corrected by subtracting the fluorescence of the sample containing only bis-ANS. The data were plotted against the total concentration of bis-ANS. The apparent K_d was estimated using the equation,

$$F = F_{max}[\text{bis-ANS}]/(K_D + \text{bis-ANS}) \quad \text{(Eq. 1)}$$

For binding analyses, TP0453 (1 or 5 μM) was incubated in 50 mM Tris (pH 7.5), 50 mM NaCl in the presence of 5 μM bis-ANS for 20 min at 22 °C. Emission spectra were collected from 400 to 600 nm; net fluorescence intensities were corrected by subtracting the fluorescence of the sample containing only bis-ANS.

Analytical Gel Filtration—Gel filtration experiments were carried out using a Superdex^{TM} 75 column on a Bio-Rad FPLC system. The column was calibrated using molecular weight standard markers (GE Healthcare). All experiments were carried out using 50 mM Tris (pH 7.5), 50 mM NaCl. Typically, 500 μl of sample was loaded on the column and run at 25 °C at a flow rate of 0.3 ml/min, with detection at 280 nm. The relative elution volume (K_{AV}) was calculated based on the equation,

$$K_{AV} = V_e - V_o/V_g - V_o \quad \text{(Eq. 2)}$$

where V_e is the elution volume, V_o is the void volume determined by elution of blue dextran 2000 kDa, and V_g is the geometric column volume.

Glutaraldehyde Cross-linking—The cross-linking of protein samples was carried out in the presence of 1% glutaraldehyde in low (50 mm Tris (pH 7.5), 100 mm NaCl) and high salt (50 mm Tris (pH7.5), 1 M NaCl) conditions. WT, $\alpha2^{I62E}$, and $\alpha8^{V249E}$ were used at a concentration of 1 μM. The molecular masses of the cross-linked products were determined by 10% SDS-PAGE and subsequent immunoblot analysis.

BN-PAGE of Native TP0453—Freshly harvested treponemes were solubilized overnight at 4 °C with 50 mM Tris (pH 7.0), 2% *n*-dodecyl β-D-maltoside (Calbiochem), and 5% protease inhibitor mixture. Before electrophoresis, lysates were cleared of detergent-insoluble material by centrifugation at 20,000 × *g* for 20 min at 4 °C. Native lysates consisting of 2.0×10^8 spirochetes were resolved in a 4–12% Bis-Tris acrylamide gel (Bio-Rad) at 4 °C using the BN-PAGE method (37, 38). The cathode buffer (50 mM Tricine (pH 7.0) and 15 mM Bis-Tris) contained 0.02% Coomassie Brilliant Blue G-250 for the first one-third of the run, after which the gel was run with fresh cathode buffer without Coomassie Brilliant Blue G-250. For the duration of the run the anode buffer consisted of 50 mM Bis-Tris (pH 7.0). Resolved lysates were transferred to a nitrocellulose membrane in 50 mM Tricine (pH 7.0) followed by immunoblotting using TP0453 antiserum.

RESULTS

TP0453 Exists in Closed and Open Conformations—As noted earlier, we previously proposed that the polypeptide moiety of TP0453 exists in membrane-integrated and -unintegrated forms (18). To obtain structures representing these hypothesized different states, we performed crystallization experiments using concentrations of β-OG ranging from 0 to 1.0%. No crys-

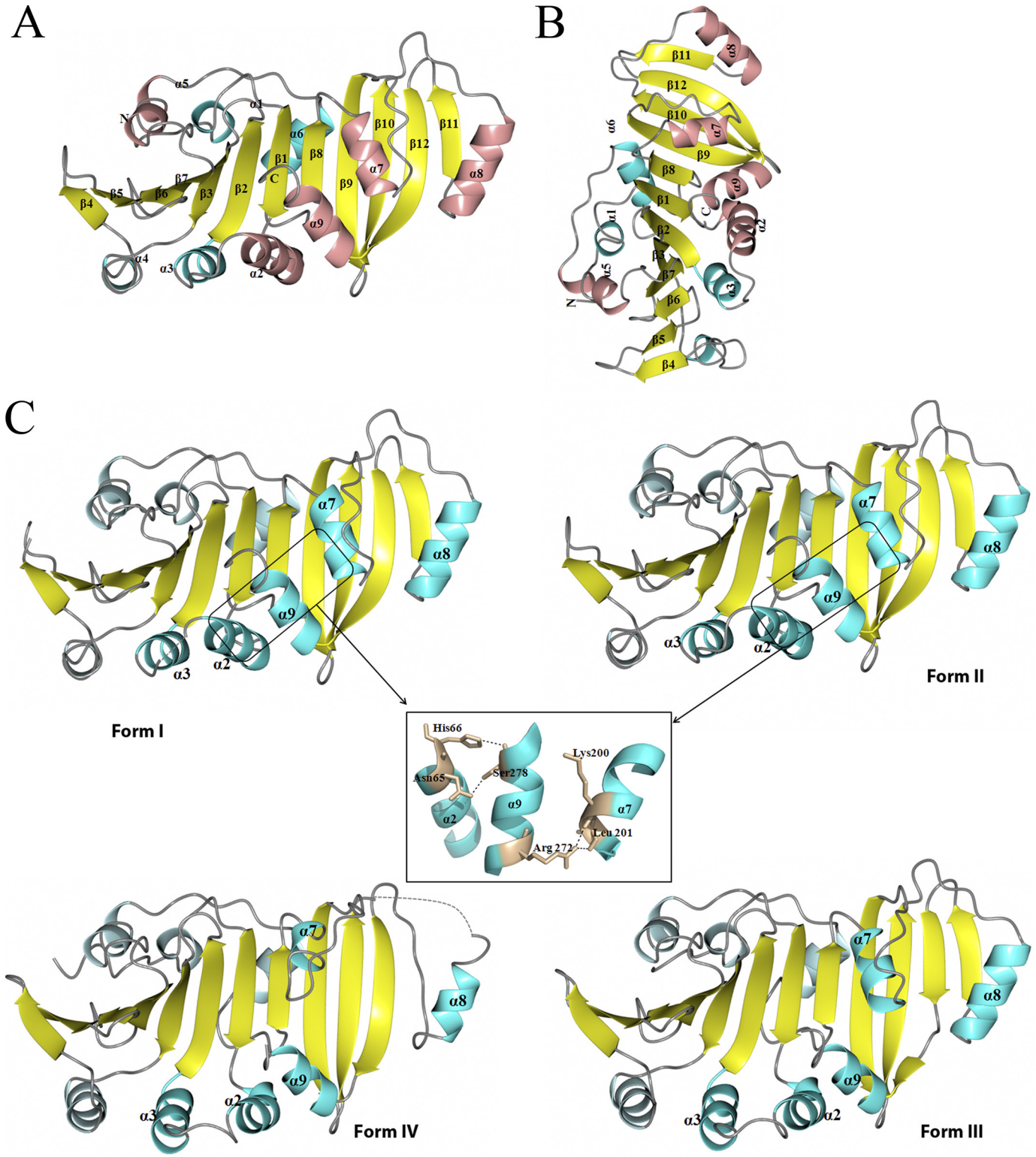

FIGURE 1. **Crystal structures of TP0453.** *A*, shown is the overall structure of TP0453 depicted as a ribbon model in which α helices are shown in *cyan* or *pink*, β strands are shown in *yellow*, and loops are shown in *gray*. Previously predicted AHs (18) are shown in *pink*. *B*, TP0453, shown in *A*, is rotated by 90° along the *z* axis. *C*, the different crystal forms of TP0453 obtained with increasing concentrations of β-OG are shown: Form I (0.1–0.25%), Form II (0.25–0.5%), Form III (0.5–0.75%), Form IV (0.75–1.0%). The helices that move are labeled and depicted in *dark cyan*. *Dotted lines* represent disordered regions in the crystal structures. The *inset* shows the hydrogen bonds which maintain the closed state but are disrupted in the open forms. The following residues are missing in the final refined structure: Form I (68 in molecule-1 and residues 63–69,104–108, and 119–120 in molecule-2), Form II (122 in molecule 1 and 119–120 in molecule 2); Form III (122), and Form IV (231–239). Otherwise, the electron densities throughout all of the polypeptide chains were high quality.

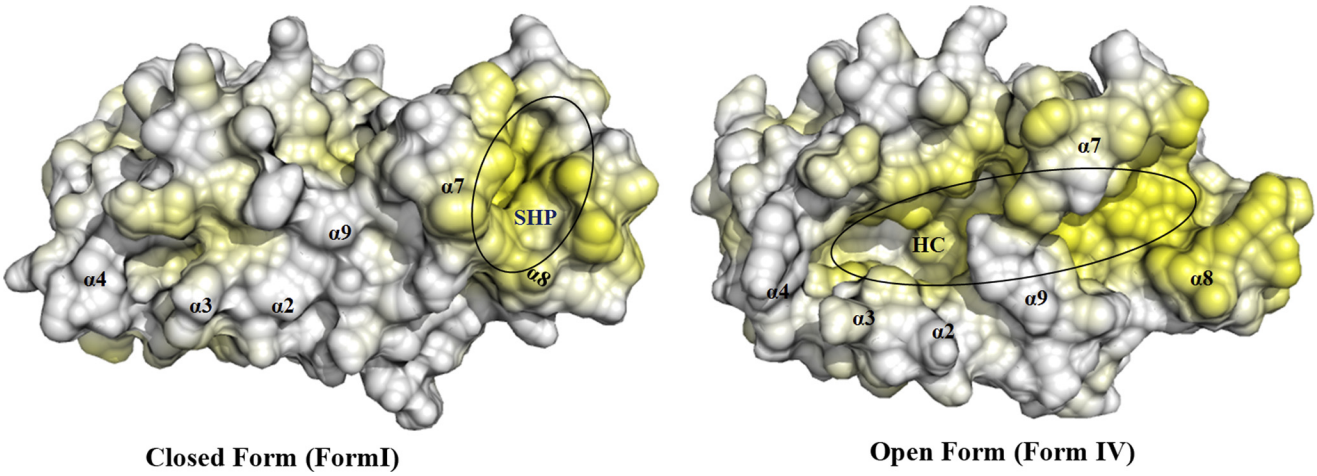

FIGURE 2. **Surface hydrophobicity of closed (*I*) and open (*IV*) forms of TP0453.** The positions of the SHP and hydrophobic cavity (*HC*) are indicated; hydrophobic residues are highlighted in *yellow*.

tals were obtained in the absence of detergent. Two forms (I and II) were obtained using 0.1–0.5% β-OG; two additional forms (III and IV, respectively) were obtained in 0.5–0.75% and 0.75–1.0% detergent. The structure of Form III was solved by multi-wavelength anomalous diffraction and refined to a resolution of 2.2 Å with R and R_{free} values of 21.2 and 26%, respectively. The structures of Forms I, II, and IV were solved by molecular replacement using Form III as a search model (see "Experimental Procedures"). The most relevant crystal parameters and refinement statistics for all crystal forms are summarized in Table 1. The final refined structures of Forms I and II contain two molecules in an asymmetric unit, whereas Forms III and IV have only one.

As shown in Fig. 1, *A* and *B*, the TP0453 structure has a globular shape with approximate dimensions of 64 × 44 × 44 Å. The overall structure of TP0453 consists of a typical α/β/α-fold consisting of a 12-stranded anti-parallel β-sheet (β1–12) sandwiched between a total of 9 α helices (α-1 to α-9). The β-sheet (strand order 11–12-10–9-8–1-2–3-7–6-5–4) forms a U-shaped β-half barrel in which strands 9, 10, and 12 are twisted in relation to the other 9 strands. Six of the nine α-helices (α2–4 and α7–9) form a lid-like structure overlying the concave face of the β-sheet, whereas three α helices (α1, α5, and α6) overlie the convex face. α2, α5, and α7–9 correspond to the AHs predicted in our previous report (18). The root mean square deviations between all C_α atoms in the four forms, depicted in Fig. 1 C, were calculated by the LSQKAB program (39) (supplemental Table 2). For comparison purposes, only molecules 1 of Forms I and II were utilized. Forms I and II are highly similar with only small deviations in the positions of α2 and α3. In contrast, a marked structural change occurs between Forms I/II and III; two groups of helices (α2/α3/α9 and α7/α8) move laterally away from each other, exposing the β-sheet, which forms the floor of a large hydrophobic cavity (calculated volume of ~3549 Å^3, Figs. 1C and 2). The transition from the closed (I/II) to open (III) form primarily involves breakage of hydrogen bonds between α7 (Lys^{200}, Leu^{201}) and α9 (Arg^{272}) and between α2 (Asn^{65}, His^{66}) and α9 (Ser^{278}) (Fig. 1*C*, *inset*). The principal change between Forms III and IV involves α7 and α8, which move outwards and away from each other, widening the mouth of the cavity and increasing the exposure of β strands 9, 10, and 12 (Fig. 1*C*). Analysis of lipophilic potential by VASCo (34) reveals that the surfaces of the closed forms contain a horseshoe-shaped hydrophobic patch (designated SHP (surface hydrophobic patch), Fig. 2) comprised of a small portion of α7 and much of α8, which is disrupted by the opening of the molecule. A DALI search (40) failed to reveal any structural homologs in the databases.

Membrane Insertion of TP0453 Occurs via α7 and α8 and Involves Surface-accessible Residues—We next conducted experiments to identify the regions of TP0453 responsible for membrane integration, turning our attention to its AHs as potential membrane insertion elements. A defining feature of AHs is that their hydrophobic and polar residues segregate to opposite faces of the helix; upon insertion into a lipid bilayer, the hydrophobic face adopts an orientation parallel to the membrane (41, 42). A helical wheel analysis using PyMOL revealed that α2, α5, and α7–9 are the only AHs in TP0453 (Fig. 3). Inspection of the TP0453 closed structures reveals that the hydrophobic faces of α2, α5, α9 are oriented toward the β sheet, whereas as noted earlier, the hydrophobic faces of both α7 and α8 contribute to varying extents to the SHP (Figs. 2 and 3). α7 and α8, therefore, appear to be the AHs most likely to be involved in membrane insertion. To examine this prediction, we generated mutant proteins in which a residue on the hydrophobic face of each AH was replaced by a glutamic acid (Fig. 3 and supplemental Table 1). No significant differences in secondary structure were observed between WT and mutants as determined by far-UV CD spectroscopy (supplemental Fig. 1). We then used Triton X-114 phase partitioning to compare the amphiphilic properties of WT and mutants. As shown in Fig. 4*A*, WT and three of the mutants (α2^{I62E}, α5^{L162E}, and α9^{I277E}) partitioned exclusively into the detergent-enriched phase; two of the mutants (α8^{V249E} and α7^{L201E}), however, showed marked deviations in phase partitioning behavior. α7^{L201E} partitioned into both aqueous and detergent phases, whereas α8^{V249E} partitioned exclusively into the aqueous phase.

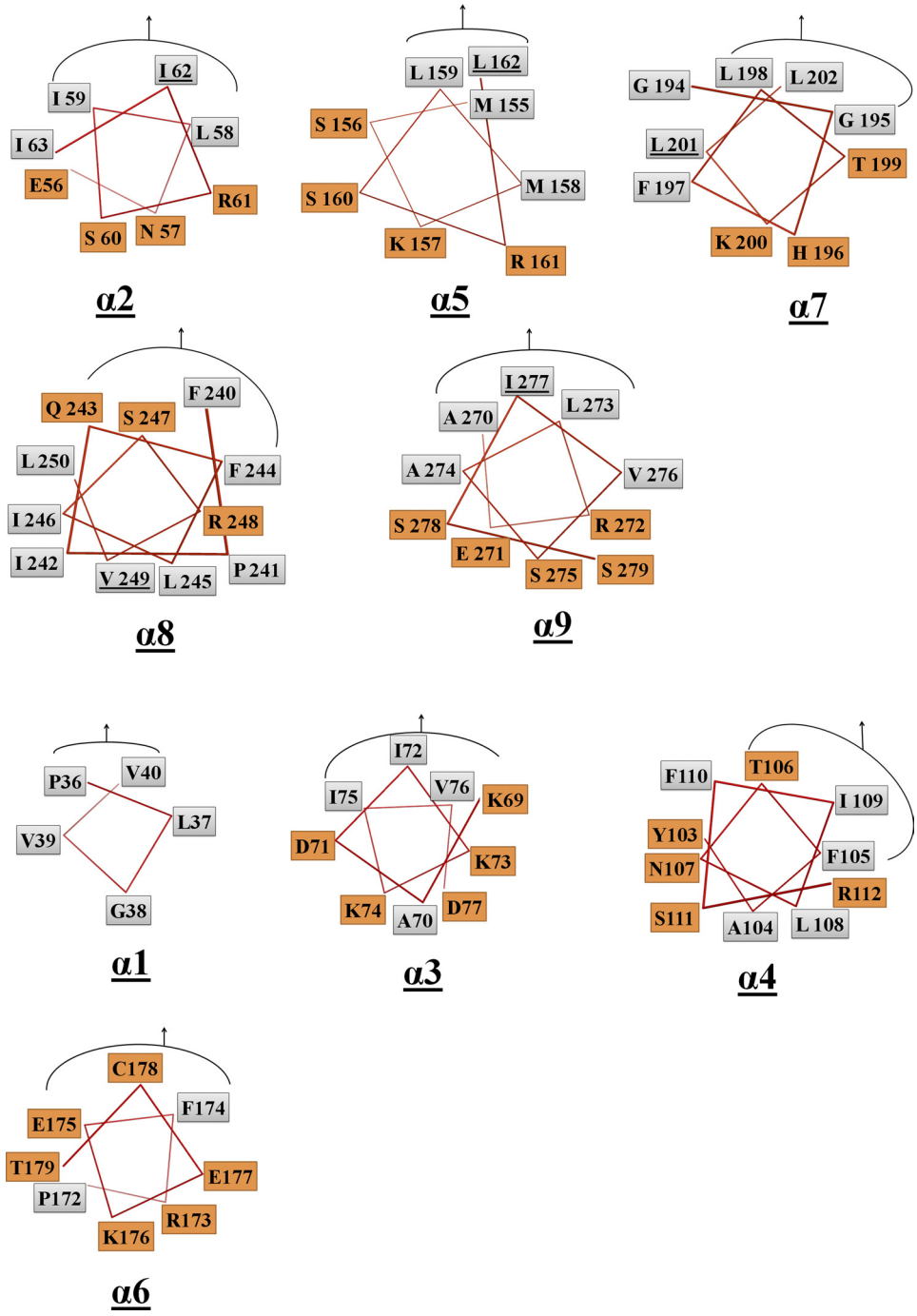

FIGURE 3. **Identification of AHs in TP0453.** PyMOL was used to construct helical wheels for all nine AHs based on the closed structures in Fig. 1. For each helical wheel, the hydrophobic and polar amino acids are shown in *gray* and *orange boxes*, respectively; the *curved line plus arrow* denotes the residues facing toward the β sheet. The five AHs (α2, α5, α7–9) indentified by this and our previous analysis are grouped together and correspond to the *pink helices* in figure 1. Residues selected for mutagenesis are *underlined*.

We extended these results using a liposome floatation assay. WT and mutant proteins were incubated with LUVs followed by discontinuous sucrose gradient centrifugation to separate membrane-associated (top fraction) from unassociated material (middle and bottom fractions); incubation under low and high salt conditions was performed to distinguish electrostatic interactions from those involving membrane integration (43). As shown in Fig. 4*B*, WT was predominantly liposome-associated under high salt, as were the same three mutants ($\alpha2^{I62E}$, $\alpha5^{L162E}$, and $\alpha9^{I277E}$) that partitioned into the Triton X-114-enriched phase. The floatation results for $\alpha7^{L201E}$ and $\alpha8^{V249E}$ in high salt mirrored their aberrant phase-partitioning behaviors; a substantial amount of $\alpha7^{L201E}$ mutant was unassociated with vesicles, whereas $H8^{V249E}$ was recovered exclusively in the bottom fraction.

Binding of bis-ANS has been used extensively to probe proteins for surface-accessible hydrophobic regions (44, 45). In aqueous buffer this compound is minimally fluorescent with an emission maximum at 525 nm but upon binding to a hydrophobic surface undergoes a marked increase in fluorescence inten-

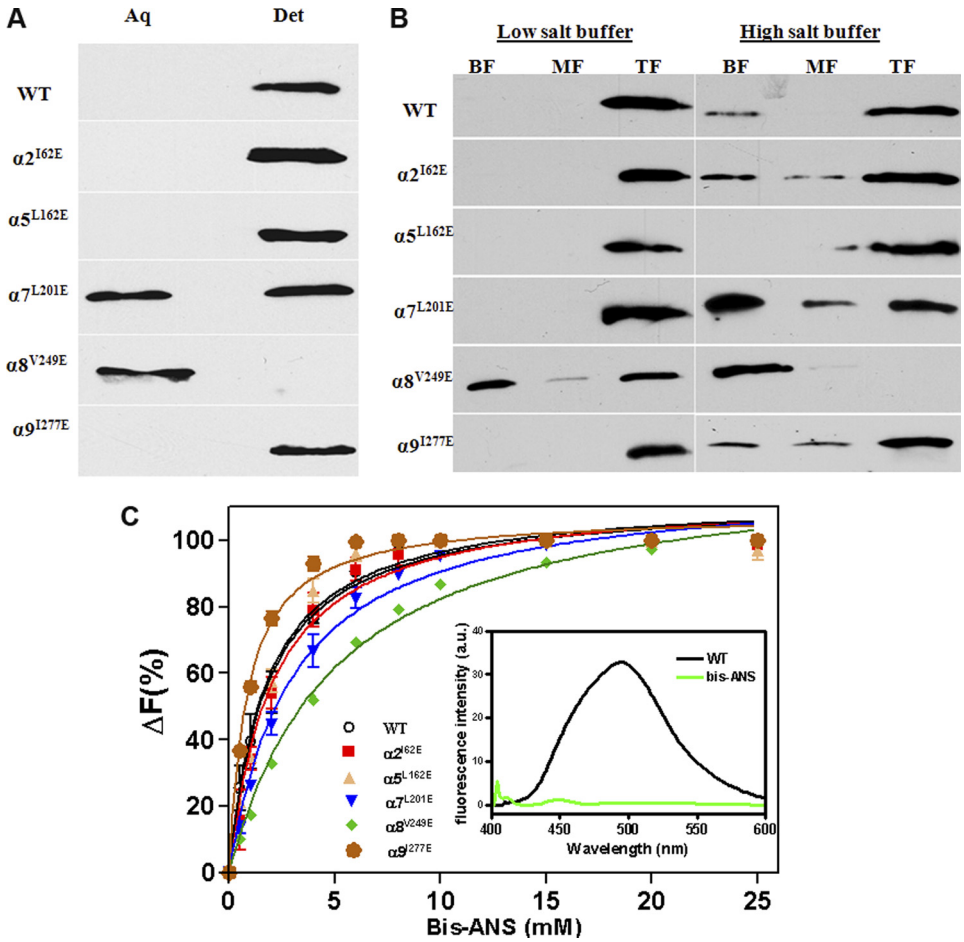

FIGURE 4. **α7 and α8 are required for membrane insertion of TP0453.** *A*, Triton X-114 phase partitioning of WT and mutants is shown. Samples were subjected to SDS-PAGE followed by immunoblotting with monospecific antiserum directed against TP0453. *aq*, aqueous; *det*, detergent. *B*, incorporation of WT and mutant proteins into LUVs is shown. *Lanes*, *bottom* (*BF*), *middle* (*MF*) and *top fractions* (*TF*) from sucrose gradients were analyzed by SDS-PAGE and immunoblotting. *C*, binding curves of WT and mutants with bis-ANS show the relative changes in fluorescence intensity at 490 nm plotted against bis-ANS concentration. The *inset* represents a fluorescence emission spectrum of WT (1 μM) or buffer alone in the presence of 1 μM bis-ANS.

TABLE 2
Bis-ANS dissociation constants (K_d) values of TP0453 and mutants

Constructs	K_d value
	μM
WT	1.792 ± 0.1939
$\alpha2^{I62E}$	2.043 ± 0.2489
$\alpha5^{L162E}$	1.723 ± 0.1746
$\alpha7^{L201E}$	2.985 ±.0.2526
$\alpha8^{V249E}$	5.047 ± 0.2486
$\alpha9^{I277E}$	0.8581 ± 0.04994

sity with a blue shift to 490 nm. Fig. 4*C* shows the binding curves for WT and mutants with increasing concentrations of bis-ANS; corresponding dissociation constants are presented in Table 2. The collective results show that bis-ANS bound well to TP0453, $\alpha2^{I62E}$, $\alpha5^{L162E}$, $\alpha9^{I277E}$, and $\alpha7^{L201E}$ but only weakly to $\alpha8^{V249E}$.

TP0453 Increases Membrane Permeability at Acidic pH—We previously demonstrated that the displacement of phospholipids after the incorporation of TP0453 into small unilamellar vesicles increases membrane permeability as measured by calcein efflux assay (18). The findings herein that only two of the protein five AHs are involved in membrane insertion prompted us to re-examine the polypeptide capacity to alter membrane permeability using a more stringent methodology involving LUVs and the fluorophore $Tb(DPA)_3^{3-}$ (46). As shown in Fig. 5, TP0453 did increase efflux of fluorophore but only at acidic pH, whereas the conventional porin, *E. coli* OmpF, increased efflux at pH 7.0.

α8 Contributes to Formation of a Membrane-inserted Dimer—Examination of the crystal lattice using the PISA program (35) indicated that Forms II, III, and IV weakly dimerize via α8 (Fig. 6*A* and supplemental Table 3). Initial experiments were conducted using size exclusion chromatography to determine whether TP0453 can form a dimer in solution. As shown in Fig. 6*B*, WT eluted in low salt buffer as a mixture of monomer and dimer. $\alpha2^{I62E}$, $\alpha5^{L162E}$, $\alpha9^{I277E}$, and α^{L201E} exhibited virtually identical elution profiles, whereas $\alpha8^{V249E}$ eluted exclusively as a monomer. These findings led us to assess whether membrane-integrated TP0453 forms dimers and whether α8 contributes to dimer formation as well as membrane insertion. WT, $\alpha2^{I62E}$, and $\alpha8^{V249E}$ were incubated in the absence and presence of LUVs under low and high salt conditions, as described for the experiments in Fig. 4*C*, followed by cross-linking with glutaraldehyde; the samples examined by SDS-PAGE and immunoblotting. The *upper* and *lower panels* of Fig. 6*C* show the results obtained, respectively, with WT and $\alpha8^{V249E}$ (not shown are the results obtained with $\alpha2^{I62E}$, which

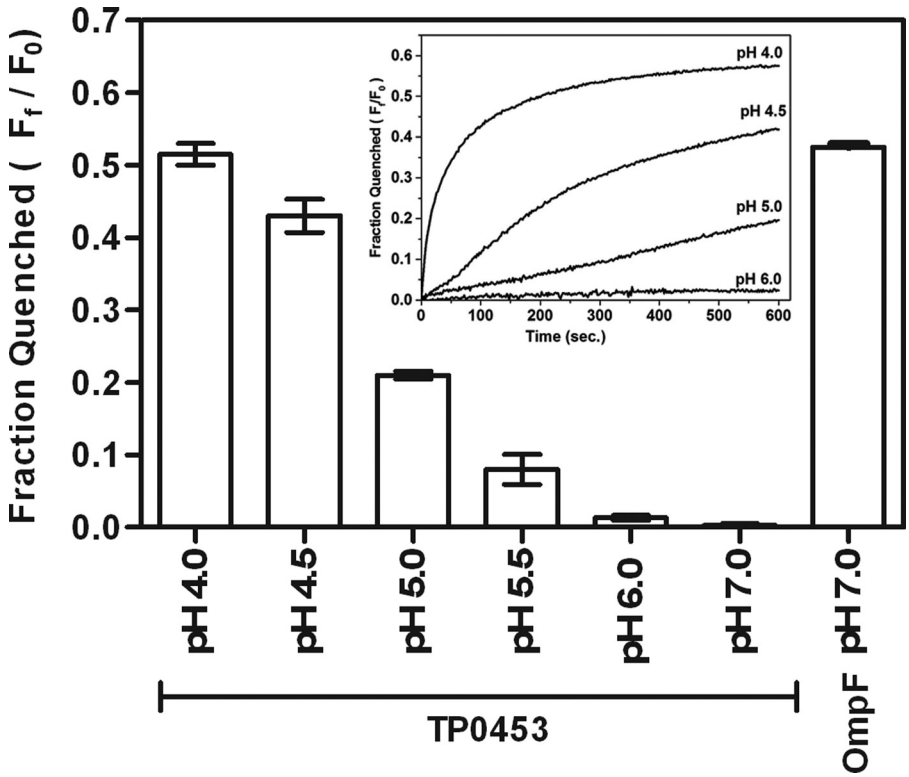

FIGURE 5. **TP0453 increases efflux of fluorophore in LUVs at acidic pH.** The graphs show pH-dependent quenching of $Tb(DPA)_3^{3-}$ from the encapsulated LUVs, after incubation with TP0453. Pore formation at pH 7.0 by *E. coli* OmpF was used as a positive control. The fractions quenched were determined as described under "Experimental Procedures." The *inset* represents initial kinetic profiles for quenching of $Tb(DPA)_3^{3-}$ from the encapsulated LUVs at different pH values.

were identical to WT). In the absence of both liposomes and glutaraldehyde, WT and $\alpha 8^{V249E}$ migrated as monomers (*lanes 1*). Cross-linking of both WT and $\alpha 8^{V249E}$ without liposomes yielded dimers (*lanes 2*) that were dissociated by high salt (*lanes 3*). However, when incubated with liposomes, cross-linked WT, but not $\alpha 8^{V249E}$, formed a dimer that was stably liposome-associated in high salt (*lanes 4* and *5*).

Last, we used BN-PAGE and immunoblot analysis to assess the relevance of these results for native TP0453. As shown in Fig. 6*D*, TP0453 in *T. pallidum* lysate migrated predominantly with a calculated molecular mass ranging from 80 to 130 kDa, a result consistent with monomer-dimer equilibrium after correcting for the approximate 50-kDa size of the *n*-dodecyl β-D-maltoside micelles (47).

DISCUSSION

In recent years an increasing number of proteins have been reported that utilize AHs as membrane anchors (48–51). The term amphitropic was coined to describe proteins whose AHs are unstructured in an aqueous milieu but adopt a helical structure upon integration into a membrane (42, 52). Previously, we postulated that the polypeptide moiety of the *T. pallidum* OM-associated lipoprotein TP0453 is amphitropic and contains five AHs that mediate reversible membrane insertion (18). Furthermore, based on our finding that membrane integration of the TP0453 polypeptide increases bilayer permeability, we hypothesized that TP0453 represents a new class of pore-forming molecule. To examine these predictions, we solved the crystal structure of non-lipidated TP0453 using graded concentrations of detergent to simulate the putative membrane-uninserted and -inserted forms of the polypeptide. The structural analysis verified the predicted AHs (α2, α5 α7–9) but also revealed that these domains are stably folded. Rather than converting between non-structured and structured forms, four AHs (α2, α7–9) were found to move during the closed to open conformational change observed with increasing concentrations of surfactant. These structural data enabled us to devise an experimental strategy to relate the membrane-interactive properties of individual AHs to the conformational changes, a key step toward elucidating the functionality of this unusual lipoprotein.

The AHs in the closed state of TP0453 exhibit two basic orientations. The hydrophobic faces of α2, α5, and α9 are oriented entirely toward the β sheet (Fig. 3), whereas portions of the hydrophobic faces of α7 and α8 face away from the β-sheet and are exposed to the aqueous milieu. The distinctive orientation of α7 and α8 suggested them as the likely membrane insertion elements. We confirmed this supposition by examining the Triton X-114 phase-partitioning behaviors and membrane interactions of mutants in which the hydrophobic faces of individual AHs were disrupted. Results obtained by probing the surfaces of WT and mutant proteins with the planar fluorescent dye bis-ANS further revealed that α8 likely functions as part of a membrane sensor that initiates the conformational changes required for membrane integration. Interestingly, we found that the same residue of α8 (Val^{249}) critical for membrane sensing/insertion is also essential for dimerization. An obvious question is whether this one helix can serve as a membrane insertion element and dimeric interface. Analysis of accessible surface area using Naccess (39) reveals that α8 does in fact contain sufficient hydrophobic surface to function

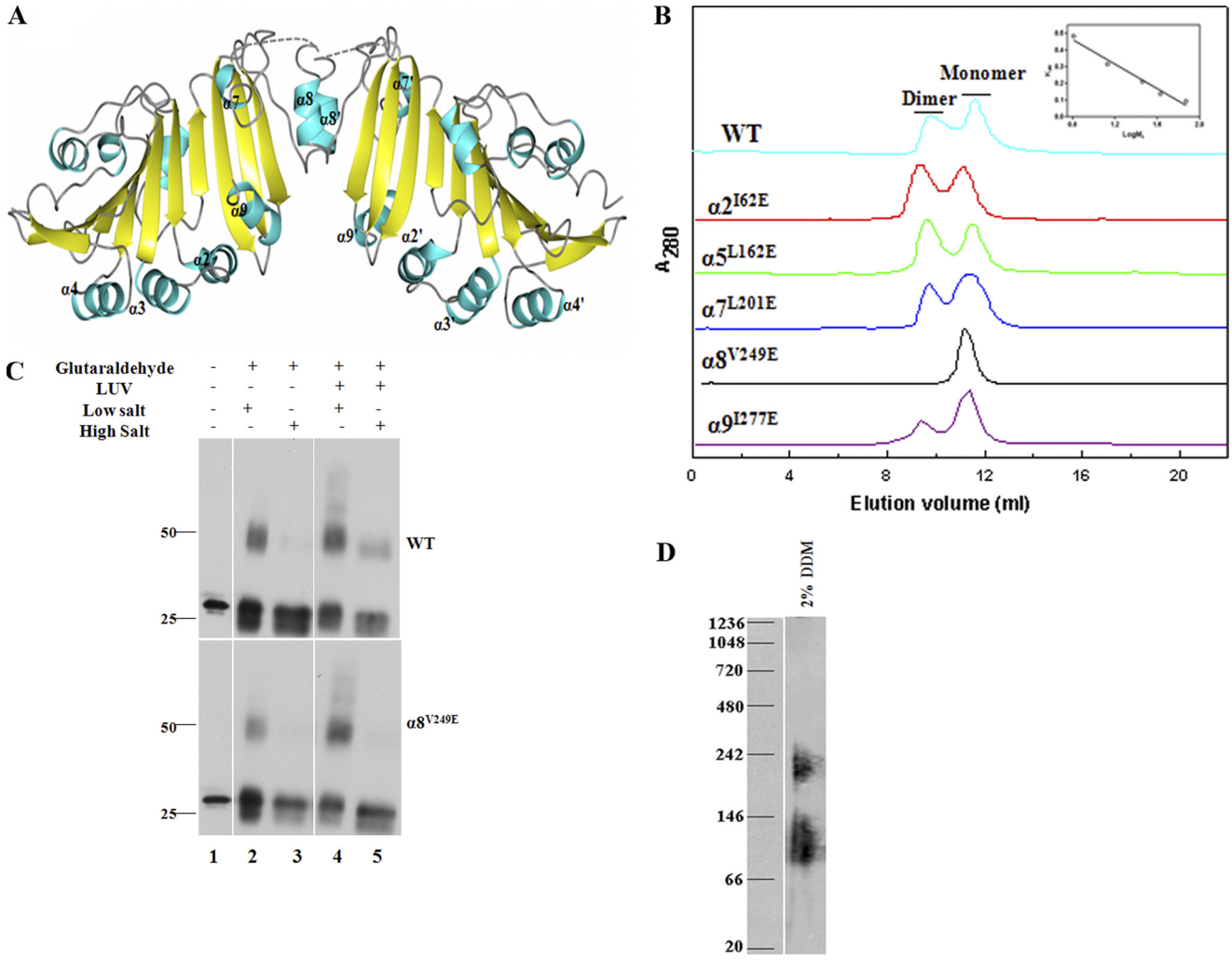

FIGURE 6. **α8 is required for dimerization as well as membrane insertion of TP0453.** *A*, shown is the dimerization mode of TP0453 predicted by the PISA server. Monomers in TP0453 assemble side-by-side along an interface established by α8. *B*, shown are elution profiles of WT and mutant proteins on a Superdex^{TM} 75 HR column in 50 mm Tris (pH 7.5), 100 mm NaCl at 25 °C. The *inset* represents the calibration curve of the column. *C*, WT, $\alpha2^{I62E}$, and $\alpha8^{V249E}$ were incubated in the absence and presence of LUVs under low and high salt conditions followed by glutaraldehyde cross-linking and SDS-PAGE/immunoblot analysis. Not shown are the results for $\alpha2^{I62E}$, which were identical to WT. *D*, shown is BN-PAGE and immunoblot analysis of *T. pallidum* lysates (2×10^8 organisms) solubilized in 2% *n*-dodecyl β-D-maltoside with 25 mM Tris (pH 7.0).

in both capacities (supplemental Fig. 2). The demonstration of a putative native dimer in *T. pallidum* supports the biologic relevance of these results.

On the basis of data presented here and elsewhere (18), it is possible to propose a scenario for membrane insertion and dimerization by the TP0453 polypeptide (Fig. 7). Initial electrostatic interactions between the charged surface of the protein and phospholipids head groups of the periplasmic leaflet would position the SHP so that it can sense transient gaps that expose the hydrophobic interior of the bilayer. In this regard it is noteworthy that TP0453 integrates more efficiently into liposomes that contain the negatively charged phospholipid, phosphatidylserine (18), a constituent of the *T. pallidum* OM (7). The energy released from the resulting hydrophobic interactions between the SHP and acyl chains within the membrane would overcome the hydrogen bonds that maintain the closed conformation, freeing α7 and α8 for insertion. Dimerization would then occur between monomers free to diffuse laterally within the lipid bilayer. It is also possible that dimerization either proceeds or occurs in parallel with membrane insertion. Significantly, the above scheme can be accommodated by our current conception of the spirochete machinery for OM localization of lipoproteins. *T. pallidum*, like Gram-negative bacteria (53), contains a Lol system for chaperoning lipoproteins across the periplasm (8, 18). Unlike cytoplasmic membrane-associated lipoproteins (*e.g.* TpN47) (5, 13), which presumably have Lol avoidance signals (53), newly exported lipidated TP0453 would be engaged by the Lol transporter (LolC, -D, and -E) (54) and subsequently transferred to the periplasmic chaperone LolA (53). *T. pallidum* does not contain an ortholog for LolB, the OM-associated lipoprotein in Gram-negative bacteria that accepts nascent lipoproteins from LolA and inserts them into the OM inner leaflet (53). The ability of the TP0453 polypeptide to spontaneously insert into membranes would, however, obviate the need for the terminal component of the Lol pathway. Lipoproteins bind to the hydrophobic cavity of LolA via their N termini; the membrane-interactive elements of TP0453 bound to LolA would, therefore, be freely accessible for interaction

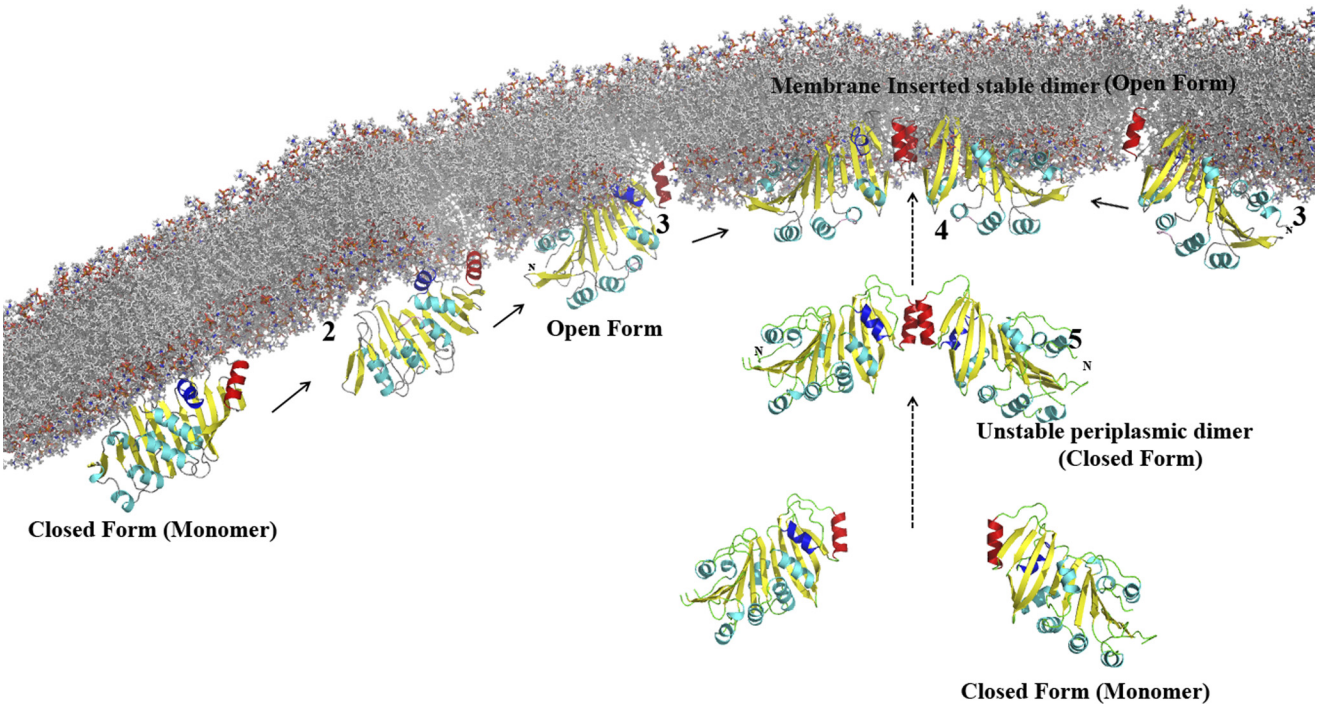

FIGURE 7. **Proposed sequence for membrane insertion and dimerization of the TP0453 polypeptide.** *1*, shown are initial electrostatic interactions between the closed form and phospholipids head groups position α7 and α8 proximal to the membrane. *2*, α7 and α8 sense transient gaps within the lipid bilayer. *3*, α7 and α8 insert into the lipid bilayer, and the molecule adopts the open conformation. *4*, adjacent membrane-inserted-monomers dimerize via α8. *5*, alternatively, monomers could dimerize before membrane sensing/insertion. In each stage, α7 and α8 are shown in *blue* and *red*, respectively.

with the periplasmic leaflet of the OM. Release of the N terminus from LolA after integration of the polypeptide would liberate the lipid moiety for insertion into the OM. Two aspects of the OM topology of TP0453 warrant emphasis (Fig. 7). First, the hydrophobic cavity of a monomer anchored to the inner leaflet by α7 and α8 would open toward the periplasmic space. Second, the positive (convex) curvature of the dimer would "match" the concavity of the OM periplasmic face.

Our earlier proposal that TP0453 functions as a pore-forming molecule was supported by results from a calcein efflux assay using small unilamellar vesicles (18). Our refined model of membrane insertion and topology prompted us to reinvestigate the molecule pore-forming properties with an alternative methodology employing LUVs, which are much less sensitive to minor perturbations (55, 56). The data obtained here demonstrate that under the physiological conditions in which membrane insertion occurs, increase in membrane permeability is not observed. Given that *T. pallidum* is an extracellular organism that is rapidly degraded within phagolysosomes (57, 58), the enhanced efflux of fluorophore observed at acidic pH is unlikely to be physiologically relevant.

Our search for an alternative function of TP0453 called our attention to the recently solved crystal structures of LprG and LppX, lipoproteins that translocate complex lipids in *M. tuberculosis* (20, 21). Both LprG and LppX contain α helices that move to accommodate large, amphipathic ligands within hydrophobic cavities delimited by β sheet (supplemental Fig. 3). The DALI server failed to identify these two lipoproteins as structural homologs because TP0453 possesses a different β-strand order and additional α-helices. Nevertheless, the structural similarities between these three molecules, readily evident upon inspection (supplemental Fig. 3), suggest that TP0453 might be a carrier of lipids, glycolipids, and/or derivatives during OM biogenesis in *T. pallidum*. TP0453 in the closed form would be unable to bind ligand during export; binding could occur, however, once the lipoprotein localizes to the OM and assumes its open conformation.

Acknowledgments—This work was based upon research conducted at the Cornell High Energy Synchrotron Source (CHESS), which is supported by the National Science Foundation under National Science Foundation Award DMR-0225180 using the Macromolecular Diffraction at CHESS (MacCHESS) facility, which is supported by National Center for Research Resources, National Institutes of Health Award RR-01646. Portions of this research were also carried out at the Stanford Synchrotron Radiation Laboratory, a national user facility operated by Stanford University on behalf of the United States Department of Energy, Office of Basic Energy Sciences. The Stanford Synchrotron Radiation Laboratory Structural Molecular Biology Program is supported by the Department of Energy, Office of Biological and Environmental Research and by the National Institutes of Health, National Center for Research Resources, Biomedical Technology Program, and the NIGMS. We acknowledge the excellent technical assistance of Morgan LeDoyt and thank Star Dunham-Ems and V. Kuruthihalli (University of Connecticut Health Center) for valuable discussions.

REFERENCES

1. Lafond, R. E., and Lukehart, S. A. (2006) *Clin. Microbiol. Rev.* **19,** 29–49
2. Cox, D. L. (1994) *Methods Enzymol.* **236,** 390–405
3. Radolf, J. D., Hazlett, K. R. O., and Lukehart, S. A. (2006) in *Pathogenic Treponemes: Cellular and Molecular Biology* (Radolf, J. D., and Lukehart, S. A., eds) pp. 197–236, Caister Academic Press, Norfolk, UK

4. Radolf, J. D. (1995) *Mol. Microbiol.* **16,** 1067–1073
5. Cameron, C. E. (2006) in *Pathogenic Treponemmes: Cellular and Molecular Biology* (Radolf, J. D., and Lukehart, S. A. eds) pp. 237–266, Caister Academic Press, Norfolk, UK
6. Belisle, J. T., Brandt, M. E., Radolf, J. D., and Norgard, M. V. (1994) *J. Bacteriol.* **176,** 2151–2157
7. Radolf, J. D., Robinson, E. J., Bourell, K. W., Akins, D. R., Porcella, S. F., Weigel, L. M., Jones, J. D., and Norgard, M. V. (1995) *Infect. Immun.* **63,** 4244–4252
8. Fraser, C. M., Norris, S. J., Weinstock, G. M., White, O., Sutton, G. G., Dodson, R., Gwinn, M., Hickey, E. K., Clayton, R., Ketchum, K. A., Sodergren, E., Hardham, J. M., McLeod, M. P., Salzberg, S., Peterson, J., Khalak, H., Richardson, D., Howell, J. K., Chidambaram, M., Utterback, T., McDonald, L., Artiach, P., Bowman, C., Cotton, M. D., Fujii, C., Garland, S., Hatch, B., Horst, K., Roberts, K., Sandusky, M., Weidman, J., Smith, H. O., and Venter, J. C. (1998) *Science* **281,** 375–388
9. Cox, D. L., and Radolf, J. D. (2001) *Microbiology* **147,** 1161–1169
10. Walker, E. M., Zampighi, G. A., Blanco, D. R., Miller, J. N., and Lovett, M. A. (1989) *J. Bacteriol.* **171,** 5005–5011
11. Desrosiers, D. C., Anand, A., Luthra, A., Dunham-Ems, S. M., LeDoyt, M., Cummings, M. A., Eshghi, A., Cameron, C. E., Cruz, A. R., Salazar, J. C., Caimano, M. J., and Radolf, J. D. (2011) *Mol. Microbiol.* **80,** 1496–1515
12. Liu, J., Howell, J. K., Bradley, S. D., Zheng, Y., Zhou, Z. H., and Norris, S. J. (2010) *J. Mol. Biol.* **403,** 546–561
13. Cox, D. L., Luthra, A., Dunham-Ems, S., Desrosiers, D. C., Salazar, J. C., Caimano, M. J., and Radolf, J. D. (2010) *Infect. Immun.* **78,** 5178–5194
14. Narita, S., Matsuyama, S., and Tokuda, H. (2004) *Arch. Microbiol.* **182,** 1–6
15. Brunner, J. (1996) *Trends Cell Biol.* **6,** 154–157
16. Shevchenko, D. V., Sellati, T. J., Cox, D. L., Shevchenko, O. V., Robinson, E. J., and Radolf, J. D. (1999) *Infect. Immun.* **67,** 2266–2276
17. Brusca, J. S., and Radolf, J. D. (1994) *Methods Enzymol.* **228,** 182–193
18. Hazlett, K. R., Cox, D. L., Decaffmeyer, M., Bennett, M. P., Desrosiers, D. C., La Vake, C. J., La Vake, M. E., Bourell, K. W., Robinson, E. J., Brasseur, R., and Radolf, J. D. (2005) *J. Bacteriol.* **187,** 6499–6508
19. Jones, J. D., Bourell, K. W., Norgard, M. V., and Radolf, J. D. (1995) *Infect. Immun.* **63,** 2424–2434
20. Sulzenbacher, G., Canaan, S., Bordat, Y., Neyrolles, O., Stadthagen, G., Roig-Zamboni, V., Rauzier, J., Maurin, D., Laval, F., Daffé, M., Cambillau, C., Gicquel, B., Bourne, Y., and Jackson, M. (2006) *EMBO J.* **25,** 1436–1444
21. Drage, M. G., Tsai, H. C., Pecora, N. D., Cheng, T. Y., Arida, A. R., Shukla, S., Rojas, R. E., Seshadri, C., Moody, D. B., Boom, W. H., Sacchettini, J. C., and Harding, C. V. (2010) *Nat. Struct. Mol. Biol.* **17,** 1088–1095
22. Gasteiger, E., Gattiker, A., Hoogland, C., Ivanyi, I., Appel, R. D., and Bairoch, A. (2003) *Nucleic Acids Res.* **31,** 3784–3788
23. Luft, J. R., Collins, R. J., Fehrman, N. A., Lauricella, A. M., Veatch, C. K., and DeTitta, G. T. (2003) *J. Struct. Biol.* **142,** 170–179
24. Koszelak-Rosenblum, M., Krol, A., Mozumdar, N., Wunsch, K., Ferin, A., Cook, E., Veatch, C. K., Nagel, R., Luft, J. R., Detitta, G. T., and Malkowski, M. G. (2009) *Protein Sci.* **18,** 1828–1839
25. Soltis, S. M., Cohen, A. E., Deacon, A., Eriksson, T., González, A., McPhillips, S., Chui, H., Dunten, P., Hollenbeck, M., Mathews, I., Miller, M., Moorhead, P., Phizackerley, R. P., Smith, C., Song, J., van dem Bedem, H., Ellis, P., Kuhn, P., McPhillips, T., Sauter, N., Sharp, K., Tsyba, I., and Wolf, G. (2008) *Acta Crystallogr. D Biol. Crystallogr.* **64,** 1210–1221
26. Otwinowski, Z., and Minor, W. (1997) in *Methods in Enzymology* (Carter, C. W., Jr., ed) pp. 307–326, Academic Press, Inc., New York
27. Sheldrick, G. M. (2010) *Acta Crystallogr D. Biol. Crystallogr.* **66,** 479–485
28. de La Fortelle, E., and Bricogne, G. (1997) in *Methods in Enzymology* (Carter, C. W., Jr., ed) pp. 472–494, Academic Press, Inc., New York
29. Morris, R. J., Perrakis, A., and Lamzin, V. S. (2003) *Methods Enzymol.* **374,** 229–244
30. Murshudov, G. N., Vagin, A. A., and Dodson, E. J. (1997) *Acta Crystallogr. D Biol. Crystallogr* **53,** 240–255
31. Emsley, P., and Cowtan, K. (2004) *Acta Crystallogr D Biol. Crystallogr.* **60,** 2126–2132
32. McCoy, A. J., Grosse-Kunstleve, R. W., Adams, P. D., Winn, M. D., Storoni, L. C., and Read, R. J. (2007) *J. Appl. Crystallogr.* **40,** 658–674
33. Winn, M. D., Isupov, M. N., and Murshudov, G. N. (2001) *Acta Crystallogr D. Biol. Crystallogr* **57,** 122–133
34. Steinkellner, G., Rader, R., Thallinger, G. G., Kratky, C., and Gruber, K. (2009) *BMC Bioinformatics* **10,** 32
35. Xu, Q., Canutescu, A. A., Wang, G., Shapovalov, M., Obradovic, Z., and Dunbrack, R. L., Jr. (2008) *J. Mol. Biol.* **381,** 487–507
36. Whitmore, L., and Wallace, B. A. (2004) *Nucleic Acids Res.* **32,** W668–W673
37. Schägger, H., and von Jagow, G. (1991) *Anal. Biochem.* **199,** 223–231
38. Wittig, I., Braun, H. P., and Schägger, H. (2006) *Nat. Protoc.* **1,** 418–428
39. Winn, M. D., Ballard, C. C., Cowtan, K. D., Dodson, E. J., Emsley, P., Evans, P. R., Keegan, R. M., Krissinel, E. B., Leslie, A. G., McCoy, A., McNicholas, S. J., Murshudov, G. N., Pannu, N. S., Potterton, E. A., Powell, H. R., Read, R. J., Vagin, A., and Wilson, K. S. (2011) *Acta Crystallogr. D Biol. Crystallogr.* **67,** 235–242
40. Holm, L., and Sander, C. (1995) *Trends Biochem. Sci.* **20,** 478–480
41. Hristova, K., Wimley, W. C., Mishra, V. K., Anantharamiah, G. M., Segrest, J. P., and White, S. H. (1999) *J. Mol. Biol.* **290,** 99–117
42. Cornell, R. B., and Taneva, S. G. (2006) *Curr. Protein Pept. Sci.* **7,** 539–552
43. Romano, F. B., Rossi, K. C., Savva, C. G., Holzenburg, A., Clerico, E. M., and Heuck, A. P. (2011) *Biochemistry* **50,** 7117–7131
44. Farris, F. J., Weber, G., Chiang, C. C., and Paul, I. C. (1978) *J. Am. Chem. Soc.* **100,** 4469–4474
45. Smoot, A. L., Panda, M., Brazil, B. T., Buckle, A. M., Fersht, A. R., and Horowitz, P. M. (2001) *Biochemistry* **40,** 4484–4492
46. Heuck, A. P., Tweten, R. K., and Johnson, A. E. (2003) *J. Biol. Chem.* **278,** 31218–31225
47. Rosevear, P., VanAken, T., Baxter, J., and Ferguson-Miller, S. (1980) *Biochemistry* **19,** 4108–4115
48. Szeto, T. H., Rowland, S. L., Rothfield, L. I., and King, G. F. (2002) *Proc. Natl. Acad. Sci. U.S.A.* **99,** 15693–15698
49. Lenarcic, R., Halbedel, S., Visser, L., Shaw, M., Wu, L. J., Errington, J., Marenduzzo, D., and Hamoen, L. W. (2009) *EMBO J.* **28,** 2272–2282
50. Marcia, M., Ermler, U., Peng, G., and Michel, H. (2009) *Proc. Natl. Acad. Sci. U.S.A.* **106,** 9625–9630
51. Dasanayake, D., Richaud, M., Cyr, N., Caballero-Franco, C., Pittroff, S., Finn, R. M., Ausió, J., Luo, W., Donnenberg, M. S., and Jardim, A. (2011) *Mol. Microbiol.* **81,** 734–750
52. Seelig, J. (2004) *Biochim. Biophys. Acta* **1666,** 40–50
53. Okuda, S., and Tokuda, H. (2011) *Annu. Rev. Microbiol.* **65,** 239–259
54. Yakushi, T., Masuda, K., Narita, S., Matsuyama, S., and Tokuda, H. (2000) *Nat. Cell Biol.* **2,** 212–218
55. Hope, M. J., Bally, M. B., Mayer, L. D., Janoff, A. S., and Cullis, P. R. (1986) *Chem. Phys. Lipids* **40,** 89–107
56. Moreira, J. N., Almeida, L. M., Geraldes, C. F., and Costa, M. L. (1996) *J. Mater. Sci. Mater. Med.* **7,** 301–303
57. Lukehart, S. A., and Miller, J. N. (1978) *J. Immunol.* **121,** 2014–2024
58. Moore, M. W., Cruz, A. R., LaVake, C. J., Marzo, A. L., Eggers, C. H., Salazar, J. C., and Radolf, J. D. (2007) *Infect. Immun.* **75,** 2046–2062